Proudman Oceanographic Laboratory

The Generic 1-D Turbulence-SPM Model

M Regener B Szilagyi H Baumert
Report No. 48 1997

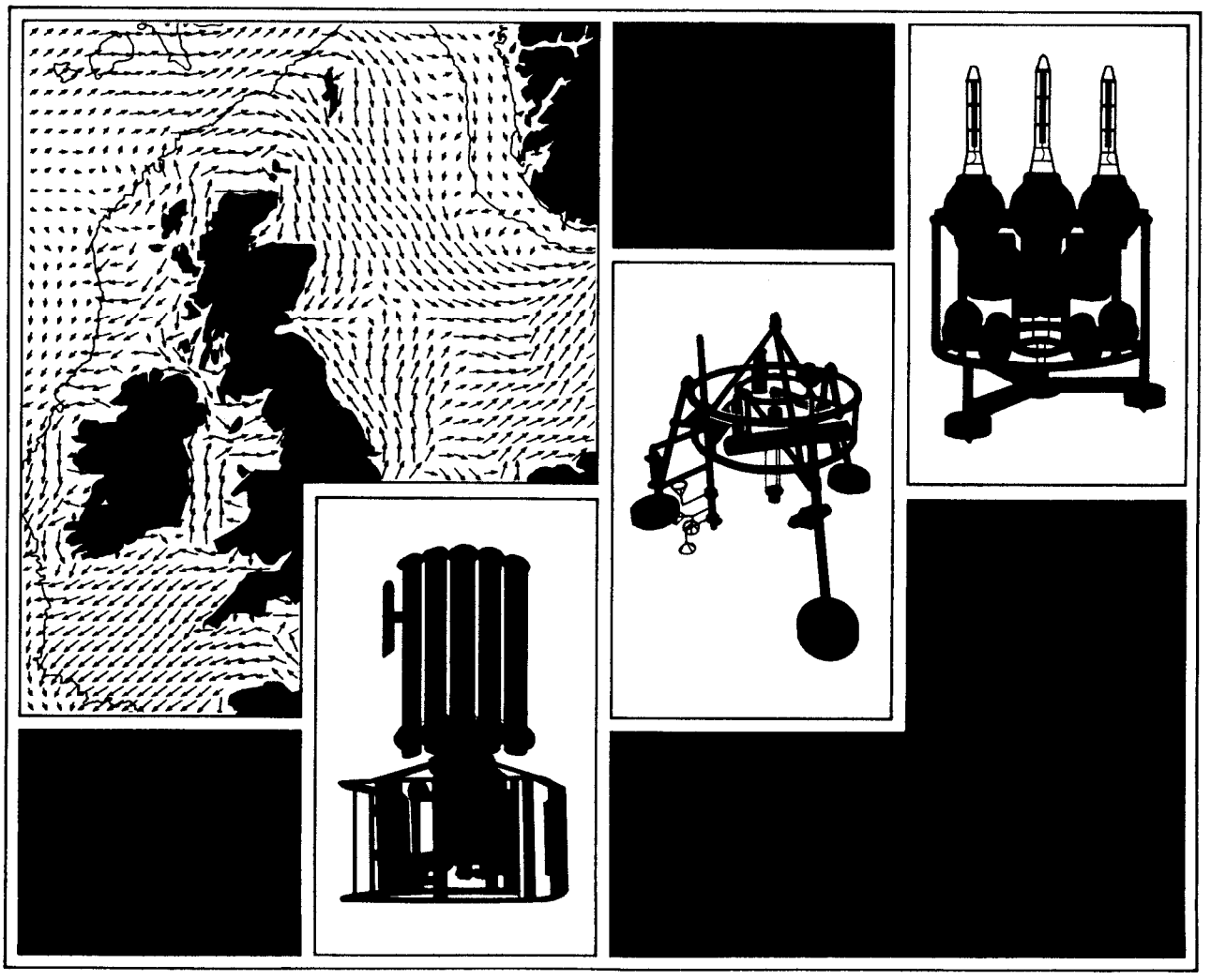

Natural Environment Research Council

PROUDMAN OCEANOGRAPHIC LABORATORY

Bidston Observatory
Birkenhead, Merseyside, L43 7RA, UK
Tel: 0151 653 8633
Telex: 628591 Ocean B
Fax: 0151 653 6269

Director: Dr. B.S. McCartney

Natural Environment Research Council

PROUDMAN OCEANOGRAPHIC LABORATORY

REPORT NUMBER 48

MAST III PROGRAMME: MAS3 CT 9500025
PROMISE
(PRe-Operational Modelling In the Seas of Europe)

The Generic 1-D Turbulence-SPM Model

M. Regener, B. Szilagyi, H. Baumert

Institut für Meereskunde
Universität Hamburg

1997

DOCUMENT DATA SHEET

AUTHOR M. Regener, B. Szilagyi and H. Baumert	PUBLICATION DATE 1997
TITLE The Generic 1-D Turbulence-SPM Model	
REFERENCE Proudman Oceanographic Laboratory, Report No. 48, 40pp & figs	

ABSTRACT

In the framework of the EU-project PROMISE one-dimensional generic turbulence-SPM-wave interaction models were derived in order to investigate the role of turbulence in relation to SPM and density stratification on a microscale in space and time. The results are being planned to improve existing multi-dimensional SPM-models on a pre-operational level.

Two versions of a one-dimensional turbulence-SPM-wave interaction model were established: Version (A) considers cohesive SPM (i.e. flocs), version (B) focuses on non-cohesive material (i.e. sand). Starting point was the k-e model as described by Baumert & Radach (1994) and Burchard & Baumert (1992). With regard to the wave influence only the tidal wave is considered in the present version.

ISSUING ORGANISATION **Proudman Oceanographic Laboratory** **Bidston Observatory** **Birkenhead** **Merseyside** **L43 7RA** **UK** **Director: Dr B S McCartney**	*TELEPHONE*: **(0151) 653 8633** *FAX:* **(0151) 653 6269** *TELEX:* **628591 OCEAN BG**

KEYWORDS MATHEMATICAL MODELS TIDAL MODELS TURBULENCE SUSPENDED PARTICULATE MATTER COHESIVE SEDIMENTS NON-COHESIVE SEDIMENTS DENSITY STRATIFICATION	*CONTRACT* *PROJECT* *MHT-75-5* *PRICE* *£13.00*

Copies of this report are available from:
The Library, Proudman Oceanographic Laboratory.

Contents

1 Introduction

Within the framework of the EU PROMISE project, 1-d generic turbulence-SPM-wave interaction models have been derived to investigate the role of turbulence in relation to SPM and density stratification in space and time. It is planned to use the results to improve existing multi-dimensional SPM models on a pre-operational level.

The starting point for the model development was the k-ε model described by *Baumert & Radach* [1994] and *Burchard & Baumert* [1995] which has been expanded to include an SPM capability. Two versions of the model have been established. Version A considers cohesive SPM (*i.e.* flocs) whereas version B focusses on non-cohesive materials (*i.e.* sand). With regard to wave activity, only the tidal wave is considered at present.

The generic model versions A and B were developed with the following background in mind:

- The working area under consideration within the PROMISE project ranges from the Holderness coastal strip and the Sylt-Rømø area to the entire North Sea.
- Over small time and space scales, the transport of non-cohesive sediments and the dynamics of moveable beds are important.
- On larger scales cohesive SPM transport and floc dynamics including autocatalytic production (cell division) of new flocs due to biological processes (to be addressed during a later phase of PROMISE) become important.

To derive the generic turbulence-SPM-wave interaction model (version A), the k-ε model has been considerably improved and extended by the inclusion of a transport module for SPM, which includes sinking and diffusion processes. At present, only a single floc size is considered. However, further development will lead to a minimum of three size classes. As version A includes only cohesive materials, the processes of erosion and sedimentation are not implemented *i.e.* there is no exchange with the bed in version A of the model. In order to be able to resolve the fluffy layer close to the bottom, we have introduced an non-uniform spatial grid.

While the k, ε, u and v model equations are solved by a fully implicit three-point, two-layer finite-difference scheme (see *Samarskij* [1984]), the

numerical solution of the SPM sinking/diffusion problem is carried out utilising the control volume method of *Patankar* [1980]. This method incorporates a power law interpolation scheme, sequential implicit time marching and deals with both smaller and larger grid Peclet numbers. The numerical diffusion inherent in the advective/sinking term is reduced by applying the Hybrid Linear/Parabolic Approximation (HLPA) introduced by *Zhu* [1991].

Version B of the model considers non-cohesive SPM and hence, in addition to the advection and diffusion processes, also includes resuspension and sedimentation processes, after *Sheng & Villaret* [1989]. It is also necessary to allow the grid to adapt to the time dependent variation in water depth (moveable bed), thus also changing the model's domain of integration.

A first test of the model was conducted for the site of the FLEX experiment [1976], from which the required meterological forcing data and measured temperature profiles for validation of the model results were available. First results showed that the characteristic features of the vertical temperature gradient are well reproduced. Furthermore, turbulent microstructure parameters showed reasonable values.

Further applications of the 1-d model are planned for the time of the PROMIX experiment as these datasets will allow detailed insight into the ability of the model to simulate the microstructure properties of turbulent flows.

2 Model Description

The model presented here is based on the k-ε turbulence model which in our case is used in its one dimensional form, including the boundary layer approximation and the earth's rotation. The coordinate system is located at mean sea level with the vertical axis directed upwards. In §2.1 we present the standard k-ε model. The SPM submodel versions A and B are presented in §2.2. We define the following abbreviations: $\partial_t := \frac{\partial}{\partial t}$, $\partial_x := \frac{\partial}{\partial x}$, $\partial_y := \frac{\partial}{\partial y}$ and $\partial_z := \frac{\partial}{\partial z}$ denoting the partial differentials with respect to time and cartesian coordinates, respectively.

The Reynolds equations of the hydro-thermodynamic submodel are

$$\left.\begin{aligned}
\partial_t \bar{u} + \partial_z \langle \tilde{u}\tilde{w} \rangle &= f\bar{v} - \tfrac{1}{\rho_0}\partial_x p, \\
\partial_t \bar{v} + \partial_z \langle \tilde{v}\tilde{w} \rangle &= -f\bar{u} - \tfrac{1}{\rho_0}\partial_y p, \\
\partial_t \bar{T} + \partial_z \langle \tilde{w}\tilde{T} \rangle &= \tfrac{1}{\rho_0 c_p}\partial_z I, \\
\partial_t \bar{S} + \partial_z \langle \tilde{w}\tilde{S} \rangle &= 0, \\
\partial_t \bar{\phi}_i + \partial_z \langle \tilde{w}\tilde{\phi}_i \rangle + w_{s,i}\partial_z \bar{\phi}_i &= \Omega_i^+ + \Omega_i^-,
\end{aligned}\right\} \qquad (1)$$

where $\bar{u}$, $\bar{v}$, $\bar{w}$, $\bar{T}$, $\bar{S}$ and $\bar{\phi}_i$ are the ensemble means of the velocity components, temperature, salinity and suspended matter (SPM, non-cohesive material in model version B and cohesive material in model version A) concentration, respectively. $\tilde{u}$, $\tilde{v}$, $\tilde{w}$, $\tilde{T}$, $\tilde{S}$ and $\tilde{\phi}_i$ represent their fluctuations. In both model versions A and B ϕ_i denotes the i'th fraction of SPM under consideration, with $i = 1..N$ and N the total number of fractions which are accounted for. Since at the moment only one floc size class is included in model version A and one SPM fraction in model version B $N = 1$ in both models. In the 1-d case the equation of continuity degenerates to $\bar{w} = 0$. $\langle \tilde{u}\tilde{w} \rangle$ and $\langle \tilde{v}\tilde{w} \rangle$ represent turbulent fluxes of momentum, ρ_0 is the mean density and p the hydrostatic pressure at the depth z, for which $p(z,t) = g\int_z^\zeta \rho\left(\bar{T}(z',t), \bar{S}(z',t), \bar{\phi}(z',t)\right) dz'$, with ζ the deviation from the mean water level. $\langle \tilde{w}\tilde{T} \rangle$, $\langle \tilde{w}\tilde{S} \rangle$ and $\langle \tilde{w}\tilde{\phi}_i \rangle$ are the turbulent fluxes of heat, salt and SPM, respectively. $w_{s,i}$ denotes the sinking velocity of the i'th SPM fraction, f is the Coriolis parameter, g the gravitational acceleration

and $\frac{1}{\rho_0}\partial_x p$ and $\frac{1}{\rho_0}\partial_y p$ represent the horizontal pressure gradients in x and y directions respectively. Since model version B deals exclusively with non-cohesive material, Ω_i^+ and Ω_i^- are defined with regard to the cohesive material in model version A only. They denote sources and sinks regarding the i'th floc size class included in model version A and represent the interaction between different floc size classes due to physical, biological and chemical processes. These processes are responsible for an increase or decrease in floc size class concentration due to coagulation of smaller flocs to bigger ones or to the breakup of bigger flocs into smaller ones.

c_p is the specific heat capacity of seawater. $\partial_z I$ represents the differential absorption of incoming radiation. In model version A the water depth is fixed to H and since changes in water depth in model version B occur stepwise rather than continous, water depth can be regarded to be constant in this case at any time step as well.

Molecular viscosity and diffusivity in (1) are neglected as they are small compared to their turbulent counterparts.

The pressure gradients are determined by the periodic sea surface elevation due to tidal action and are modelled as follows:

$$\left.\begin{aligned} -\tfrac{1}{\rho_0}\partial_x p = -g\partial_x \zeta &= A_{x,m}\sin[\omega_m t + \phi_m] \\ &+ A_{x,s}\sin[\omega_s t + \phi_s] \end{aligned}\right\} \tag{2}$$

and

$$\left.\begin{aligned} -\tfrac{1}{\rho_0}\partial_y p = -g\partial_y \zeta &= A_{y,m}\cos[\omega_m t + \phi_m] \\ &+ A_{y,s}\cos[\omega_s t + \phi_s] \end{aligned}\right\} \tag{3}$$

In equations (2) and (3), $A_{i,j}$ represent the amplitudes ($i = x, y$; $j = m, s$) of lunar and solar tidal components with s and m referring to the solar and lunar components. ω_m, ω_s and ϕ_m, ϕ_s denote their angular frequencies and phases respectively

Due to the unknown correlators $< .. >$, (1) does not represent a closed system of equations. It is necessary to introduce some assumptions regarding the turbulent fluxes of material, momentum and heat. The computation of these fluxes is described below.

2.1 The k-ε Model

Within the k-ε model, the turbulent kinetic energy (TKE) and dissipation rate of TKE (ε) are described via transport equations. TKE and ε are defined by

$$k = \frac{1}{2}(\langle\tilde{u}^2\rangle + \langle\tilde{v}^2\rangle + \langle\tilde{w}^2\rangle) \tag{4}$$

and

$$\varepsilon = \nu \sum_j \sum_i \langle(\partial_j \tilde{v}_i)^2\rangle, \tag{5}$$

($i = x, y, z$; $j = x, y, z$) where tilded quantities denote fluctuations and ν is the molecular viscosity. Equations (4) and (5) allow us to describe the temporal and spatial variability of the turbulent dynamics of the water coloumn in detail. Exact transport equations for these quantities can be derived from the Navier–Stokes and the Reynolds equations. However, they contain again, as in (1) unknown higher-order correlators which have to be described by closure assumptions.

In its final form, the k-ε model is given by (cf. *Rodi* [1980]):

$$\partial_t k + \mathit{Diff}(k) = P + G - \varepsilon \tag{6}$$

$$\partial_t \varepsilon + \mathit{Diff}(\varepsilon) = c_1(P + c_3 G)\frac{\varepsilon}{k} - c_2\frac{\varepsilon^2}{k} \tag{7}$$

where

$$P = -\langle\tilde{u}\tilde{w}\rangle\partial_z\bar{u} - \langle\tilde{v}\tilde{w}\rangle\partial_z\bar{v} \tag{8}$$

is the shear production and

$$G = -\frac{g}{\rho_0}\langle\tilde{w}\tilde{\rho}\rangle \tag{9}$$

is the buoyancy production of TKE. The "*Diff*" diffusion terms in (6) and (7) are specified later. The density ρ is a function of temperature and salinity. The mean and fluctuating density are approximated by

$$\begin{aligned} \langle\rho(T,S,\phi)\rangle = \langle\rho(\bar{t}+\tilde{T},\bar{S},\bar{\phi})\rangle &\approx \rho(\bar{T},\bar{S},\bar{\phi}) \\ \tilde{\rho} := \rho(T,S,\phi) - \langle\rho(T,S,\phi)\rangle &\approx \tilde{T}\partial_T\rho(\bar{T},\bar{S},\bar{\phi}), \end{aligned} \tag{10}$$

i.e. fluctuations in S and ϕ are neglected here. Equations (6)-(9) represent the kernel of the k-ε model.

To close the system of equations (6)-(9), the eddy viscosity concept is applied, relating the turbulent fluxes of momentum and heat to the gradients of the mean quantities *i.e.*

$$\langle \tilde{u}\tilde{w} \rangle = -\nu_t \partial_z \bar{u}, \quad \langle \tilde{v}\tilde{w} \rangle = -\nu_t \partial_z \bar{v} \tag{11}$$

and

$$\langle \tilde{w}\tilde{T} \rangle = -\frac{\nu_t}{\sigma_t}\partial_z \bar{T}, \quad \langle \tilde{w}\tilde{S} \rangle = -\frac{\nu_t}{\sigma_S}\partial_z \bar{S}, \quad \langle \tilde{w}\tilde{\phi} \rangle = -\frac{\nu_t}{\sigma_\phi}\partial_z \bar{\phi}. \tag{12}$$

The parameter ν_t represents the eddy (turbulent) viscosity. σ_t denotes the turbulent Prandtl number which is defined as the ratio of eddy viscosity to turbulent heat conductivity. σ_S and σ_ϕ are the turbulent Schmidt numbers for the transport of salt and SPM and are defined as the ratio of eddy viscosity to the appropriate eddy diffusivity.

The turbulent Prandtl number σ_t, can be modelled empirically, as described by *Munk and Anderson* [1948]

$$\sigma_t = \begin{cases} \frac{(1+\frac{10}{3}R_g)^{3/2}}{(1+10R_g)^{1/2}} & \text{for } R_g \geq 0, \\ 1, & \text{for } R_g < 0 \end{cases} \tag{13}$$

where R_g is the gradient Richardson number[1], a dimensionless measure of stratification, given by

$$\left.\begin{aligned} R_g &:= \tfrac{N^2}{S^2} \\ N^2 &:= -\tfrac{g}{\rho_0}\partial_z \rho \\ S^2 &:= (\partial_z \bar{u})^2 + (\partial_z \bar{v})^2 \end{aligned}\right\} \tag{14}$$

where S and N are the shear and Brunt–Väisälä frequencies respectively. Another important measure of the stability of stratification is provided by the flux Richardson number

$$R_f := \frac{R_g}{\sigma_t} \tag{15}$$

[1]The gradient and flux Richardson numbers are positive for stable, negative for unstable and zero for neutrally stratified flows

i.e. $R_f = -G/P$. The Kolmogorov-Prandtl relation (cf. *Kolmogorov* [1942], *Prandtl* [1945]) links the mean flow equations to the state variables of the turbulence model. This relation reads:

$$\nu_t = c_\mu \frac{k^2}{\varepsilon} \tag{16}$$

Finally, the diffusion terms for k and ε are related to the corresponding gradients thus

$$Diff(k) = -\partial_z(\frac{\nu_t}{\sigma_k}\partial_z k), \quad Diff(\varepsilon) = -\partial_z(\frac{\nu_t}{\sigma_\varepsilon}\partial_z \varepsilon). \tag{17}$$

The empirical constants used in this model are shown in Table 1 (*Rodi* [1980]). The parameter c_3 is discussed later.

c_μ	c_1	c_2	σ_k	σ_ε
0.09	1.44	1.92	1.0	1.3

Table 1: Empirical constants for the standard k-ε model

2.1.1 The Homogeneous Shear Layer

In the idealised case of a homogeneous shear layer, all diffusive terms Diff(k) and Diff(ε) in (6) and (7) are neglected, whereas the gradients in the source and sink terms P and G are not. In this case the following system of ordinary differential equations is obtained:

$$\dot{k} = \gamma_1 \frac{k^2}{\varepsilon} - \varepsilon \tag{18}$$

and

$$\dot{\varepsilon} = c_1 \gamma_2 k - c_2 \frac{\varepsilon^2}{k} \tag{19}$$

with

$$\gamma_1 = c_\mu\{(\partial_z \bar{u})^2 + (\partial_z \bar{v})^2\} + \frac{g}{\rho_0} c'_\mu \partial_z \rho \tag{20}$$

and

$$\gamma_2 = c_\mu\{(\partial_z\bar{u})^2 + (\partial_z\bar{v})^2\} + c_3\frac{g}{\rho_0}c'_\mu\partial_z\rho \tag{21}$$

with $c'_\mu := c_\mu/\sigma_t$ in the case of the standard model. With the replacement $X := \varepsilon/k$ it follows that

$$\dot{X} = \frac{k\dot{\varepsilon} - \varepsilon\dot{k}}{k^2} \tag{22}$$

with which equations (18) and (19) condense into one:

$$\dot{X} = a - bX^2 \tag{23}$$

with $a := c_1\gamma_2 - \gamma_1$ and $b := c_2 - 1 > 0$.

2.1.1.1 The Lower Limit for R_f It is obvious that the parameter b in equation (23) is a positive constant so that negative values of the function $a(t)$ may lead, under certain circumstances, to negative values of X. This is physically not permissible, because by definition ε and k are positive[2]. In order to ensure the positivity of X, the condition $a(t) \geq 0$ is sufficient (not necessary). This condition implies that

$$\begin{aligned} &R_f \geq R_f^{lim}, \text{for} \quad c_3 < \frac{1}{c_1} \\ \text{or} \qquad & \\ &R_f \leq R_f^{lim}, \text{for} \quad c_3 > \frac{1}{c_1} \end{aligned} \tag{24}$$

where R_f^{lim} represents a limiting flux Richardson number,

$$R_f^{lim} = \frac{c_1 - 1}{c_1 c_3 - 1} \tag{25}$$

which, in the present k-ε model forms a lower limit for R_f:

$$R_f \geq R_f^{lim} = \frac{c_1 - 1}{c_1 c_3 - 1} \tag{26}$$

Because of (24), this implies an upper bound for the parameter c_3, *i.e.*, $c_3 < c_1^{-1} = 0.694$. For the case of $c_3 = -1.4$ this gives $R_f^{lim} = -0.146$ (see *Burchard & Baumert* [1995]). .

[2]Negative values of ε in the sense of *Weinstock* (J. Atmosph. Sci. 37, 1980, p.1548) in relation to spectral considerations are not considered here.

2.1.1.2 The Steady State. The search for stationary solutions of the system of equations (18)-(19) leads to the following necessary relation:

$$\gamma_1 c_2 - \gamma_2 c_1 = 0 \tag{27}$$

For $\partial_z \bar{u} \neq 0$ this can be expressed through the condition:

$$R_f = R_f^{st} \tag{28}$$

where for the stationary Richardson number the following relation is valid:

$$R_f^{st} := \frac{c_2 - c_1}{c_2 - c_1 c_3} \geq R_f^{lim} \tag{29}$$

Hereby a functional relationship between the flux Richardson number and c_3 is introduced.

Consider the special case of quasi-stationary velocity and density gradients *i.e.* $\partial_t \partial_z \bar{u} = \partial_t \partial_z \rho = 0$. This is permissible since the characteristic timescales of these quantities are much larger than k/ε, the timescale of the turbulent motion.

From equation (23), it is obvious that in the case of $a \geq 0$

$$X^{-1} = \frac{k}{\varepsilon} \longrightarrow \sqrt{\frac{b}{a}} = \sqrt{\frac{c_2 - 1}{c_1 \gamma_2 - \gamma_1}} \tag{30}$$

is valid for any Richardson number. The expression $\sqrt{b/a}$ can be interpreted as the turbulent lifetime, which is established by the gradients in the mean flow.

The system (18)-(19) will be in steady state if the ration k/ε has reached its upper limit. In this case $k_\infty/\varepsilon_\infty = \gamma_1^{-1/2}$.

From equations (26)-(28), one can derive a relation between the critical numbers R_f^{st} and R_f^{lim}

$$R_f^{st} = \frac{\alpha_R R_f^-}{R_f^- - \beta_R} \tag{31}$$

with

$$\alpha_R = \frac{c_2 - c_1}{c_2 - 1} = 0.522, \quad \beta_R = \frac{c_1 - 1}{c_2 - 1} = 0.478 \tag{32}$$

The values given in equation (32) are calculated using the constants in Table 1.

For the system of equations (18)-(19), one can find analytical solutions and proofs that R_f^{lim} represents the limit for the onset of convection and R_f^{st} the limit for the collapse of turbulence (*Burchard & Baumert* [1995]).

2.1.2 Boundary Conditions

The surface and botom boundary conditions for the system of equations (1) were formulated in the usual way with the turbulent fluxes of energy and matter taken to be proportional to the vertical gradients of the appropriate property.

2.1.2.1 The Momentum Equation

1. Free Surface Boundary Condition:

$$[\nu_t \partial_z \bar{u}]_{z=0} = \frac{\tau_{xs}(t)}{\rho_0} \tag{33}$$

and

$$[\nu_t \partial_z \bar{v}]_{z=0} = \frac{\tau_{ys}(t)}{\rho_0} \tag{34}$$

with

$$\tau_{is} = \rho K_M \partial_z W_i, \quad i = x, y \tag{35}$$

K_M is the turbulent viscosity regarding the turbulent flux of momentum in the air and (W_x, W_y) is the near surface wind velocity vector. Assuming a logarithmic velocity profile, the calculation of the surface momentum flux is approximated by

$$\begin{aligned} \tau_{xs} &= c_d \rho_a W_x \sqrt{W_x^2 + W_y^2} \\ \tau_{ys} &= c_d \rho_a W_y \sqrt{W_x^2 + W_y^2} \end{aligned} \tag{36}$$

ρ_a is the air density and c_d is a wind friction coefficient that is a function of wind velocity. For wind velocities between 8 and $25 ms^{-1}$, $c_d = (1.2 + 0.025\,|W|)$ with additional formulae for other wind speeds. The coefficient c_d can be calculated using empirical formulae, for example those developed by *Kondo* [1975] which we used here.

2. Bottom Boundary Conditions:

   In order to obtain bottom boundary conditions, a logarithmic boundary layer (LBL) is assumed in which the shear stress is constant and equal to the bottom stress. Because of the strong velocity and dissipation rate gradients within the LBL, the integral mean over the bottom interval of the discrete scheme were taken as boundary conditions.

$$[\nu_t \partial_z \bar{u}]_{z=z_b} = \langle \tilde{u}\tilde{w} \rangle = -\frac{\tau_{xb}(t)}{\rho_0} = -R\bar{u}(z_b,t)u_b \tag{37}$$

   and

$$[\nu_t \partial_z \bar{v}]_{z=z_b} = \langle \tilde{v}\tilde{w} \rangle = -\frac{\tau_{yb}(t)}{\rho_0} = -R\bar{v}(z_b,t)u_b \tag{38}$$

   where $\bar{u}_b = \bar{u}(z_b,t)$ $(z_b \in LBL)$ with the layer-integrated bottom drag coefficient R given by (*e.g. Tennekes & Lumley* [1972])

$$R = \frac{\kappa^2}{ln^2[(29.96/e)(1+(1/p))^{1+p}]}, \qquad p := \frac{\mathcal{K}_S}{\Delta z} \tag{39}$$

   In equation (39) $\kappa = 0.4$ is the Kármán constant, $\mathcal{K}_S$ denotes the linear size of the roughness elements, $u_b = \sqrt{[\bar{u}(z_b,t)]^2 + [\bar{v}(z_b,t)]^2} \geq 0$ represent a mean value over the LBL and Δz the spacing of the bottom grid interval.

2.1.2.2 The Heat Balance

1. Free Surface Boundary Condition:

$$\left[\frac{\nu_t}{\sigma_t}\partial_z \bar{T}\right]_{z=0} = \frac{1}{c_p \rho_0}(Q_L + Q_S + Q_R) \tag{40}$$

   where Q_L denotes the latent heat, Q_S is the sensible heat or direct heat flux and Q_R is the heat loss due to longwave backradiation at the sea surface.

   Temperature changes due to the absorption the visible part of solar radiation are included in the source term $\frac{1}{\rho_0 c_p}\partial_z I$ in the third equation in (1), where the absorption of the longwave range of insulation at the

sea surface ($z = 0$) is given by the surface flux $\partial_t \bar{T}|_{z=0} = \frac{1}{\rho_0 c_p} I^{IR}$. I^{IR} is the insulation at the sea surface in Wm^{-2}. Obviously $I^{IR} + I(z = 0)$ denotes the total global radiation.

2. Bottom Boundary Condition:

   At the bed the adiabatic boundary condition is applied so that

$$\left[\frac{\nu_t}{\sigma_t}\partial_z \bar{T}\right]_{z=-H} = 0 \tag{41}$$

Calculation of the heat fluxes Q_L, Q_S and Q_R is carried out using empirical bulk formulae (see *Busch* [1977], *Friedrich et al.* [1981]) which are derived and presented in detail by *Kondo* [1975]. These formulae contain much empirical information such as the dependency on air density or water vapour pressure (the Magnus formula) and the effect of temperature on the specific heat of water (see *Möller* [1973]). These formulae have been applied and presented in compressed form by *Regener* [1992]. They also take into consideration the state of the atmosphere (unstable, neutral, stable). The long wave back radiation budget is calculated (*Kondratyev* [1969]) from the Stefan-Boltzman constant, the emissivity and the cloudiness (measured in Okta).

The absorption of incoming visible solar radiation is parameterised using the approach adopted by *Paulson & Simpson* [1977].

2.1.2.3 Salinity Equation For salinity the no-flux condition is assumed to hold both at the free surface and at the bottom boundary. The free surface condition is justified since precipitation and evaporation are of similar magnitude for the area of the North Sea. Thus, the boundary conditions for salt read

$$\left[\frac{\nu_t}{\sigma_S}\partial_z \bar{S}\right]_{z=0,-H} = 0 \tag{42}$$

2.1.2.4 Turbulent Kinetic Energy (TKE)

1. Free Surface Boundary Condition:

$$\left.\begin{array}{rcl} \left[\frac{\nu_t}{\sigma_k}\partial_z k\right]_{z=0} = 0, & : & if \quad k > u_s^{*2}/\sqrt{c_\mu} \\ k = u_s^{*2}/\sqrt{c_\mu} & : & \text{otherwise} \end{array}\right\} \tag{43}$$

u_s^* is the wind friction velocity at the sea surface with $u_s^* = \sqrt{\frac{\tau_s}{\rho_0}}$ and $\tau_s = \sqrt{\tau_{xs}^2 + \tau_{ys}^2}$. This approach was suggested by *Rodi* [1980]. The discrete form of (43) which is used in the model is described in chapter 3.4.

2. Bottom Boundary Condition:

$$k(z_b, t) = k(t) = [u_b^*(t)]^2 / \sqrt{c_\mu}. \tag{44}$$

2.1.2.5 The Dissipation Rate Of TKE

1. Surface Boundary Condition:

$$\epsilon = \frac{k^{3/2} c_\mu^{3/4}}{\kappa \left[z + 0.07H\left(1 - u_s^{*2}/kc_\mu^{1/2}\right)\right]} \tag{45}$$

This approach is also described by *Rodi* [1980].

2. Bottom Boundary Condition:

$$\epsilon(z_b, t) = [u_b^*(t)]^3 \frac{1}{\kappa z_b} \tag{46}$$

where u_b^* is the bottom friction velocity given by: $u_b^* = \sqrt{r(\bar{u}_b^2 + \bar{v}_b^2)}$ with $\tau_b = \frac{\sqrt{\tau_{xb}^2 + \tau_{yb}^2}}{\rho_0} = (u_b^*)^2$. Note that τ_b as well as u_b^* are constant throughout the LBL (constant stress region).

As with the momentum boundary condition equation, the TKE and dissipation equations are taken in their integral mean form over the bottom interval of the discrete scheme.

2.2 SPM Model (Version A, cohesive material)

This version of the generic model considers cohesive SPM *i.e.* flocs. Thus, besides the interaction between particles of different floc size classes, the material is assumed not to react with the bed sediments and to be continuously in suspension, with highly variable concentrations, leading to formation of a lutocline or fluffy layer and giving rise to colliding of particles of different floc size classes. The flocs are transported both up and down the water column via turbulent diffusion with settling under gravity also contributing to the downward flux. Given that there is no interaction with the bed, no-flux boundary conditions are appropriate for both bed and surface. The resulting conditions for the SPM equation in (1) are (note that in the following i, j, l mark the corresponding floc size classes)

1. Free Surface Boundary Condition:

$$\left[\bar{\phi}_i w_{s,i} - \frac{\nu_t}{\sigma_{\phi_i}} \partial_z \bar{\phi}_i\right]_{z=0} = 0. \tag{47}$$

2. Bottom Boundary Condition:

$$\left[\bar{\phi}_i w_{s,i} - \frac{\nu_t}{\sigma_{\phi_i}} \partial_z \bar{\phi}_i\right]_{z=-H} = 0. \tag{48}$$

The sinking velocity $w_{s,i}$ is dependent on the floc concentration in order to allow for so-called hindered settling. This phenomenon is observed if floc concentrations reach a critical value and there is interaction via differential settling. Beyond this critical concentration, the effective settling velocity is reduced (*van Rijn* [1993]). In order to allow for this modification in $w_{s,i}$, we have implemented the following formula due to *Oliver* [1961]:

$$w_{s,i} = (1 - 2.15 \cdot c_{\phi_i}) \cdot (1 - 0.75 \cdot c_{\phi_i}^{0.33}) \cdot w_{s,i}^0. \tag{49}$$

In equation (49), c_{ϕ_i} is a dimensionless ratio of the local instantaneous floc concentration $\bar{\phi}_i$ and a certain maximum concentration ϕ_i^* *i.e.* $c_{\phi_i} = \bar{\phi}_i / \phi_i^*$. w_s^0 is the corresponding settling velocity in clear water.

Another observed phenomenon which has to be included in the model is the influence of floc concentration on the density of seawater. Because of this, high floc concentrations can affect the hydrodynamics of the flow. High floc concentrations near the bed establish sharp concentration gradients

and corresponding vertical density gradients, especially when turbulence is weak. Because of this, turbulent motion in the bottom layer may eventually be suppressed (*Sheng & Villaret* [1989]), so that within the boundary layer further erosion due to turbulent motion will stop. This sharp density gradient will be eventually breaked up by a subsequent sufficient increase in near bed horizontal velocity components. In the model this process is considered using the following formula (*e.g Sheng & Villaret* [1989]).

$$\rho_m = c_{\phi_i} \cdot \rho_s + (1 - c_{\phi_i}) \cdot \rho \tag{50}$$

In equation (50), ρ_m is the modified density, ρ_s is the sediment density and c_{ϕ_i} the normalised SPM concentration. ρ denotes the density of sea water.

The source and sink terms Ω_i^+ and Ω_i^- in (1) are defined as the rate of change of the considered floc size class:

$$\Omega_i^+ = [\partial_t \bar{\phi}_i]^+ \qquad \text{and} \qquad \Omega_i^- = [\partial_t \bar{\phi}_i]^-, \tag{51}$$

and can be become effective only if either particles of different floc size classes get in contact or external forces (*e.g.* due to shear stress) act on the particles of the considered floc size class.
Three mechanisms are generally considered to be responsible for particle-particle contact (*Jackson* [1995]): The Brownian diffusion, laminar and turbulent shear and differential sinking. On these occasions of particle-particle contact or the acting of external forces particles can aggregate or disaggregate, respectively (*e.g.Kiørboe et al.* [1994]).

Under the assumption that only single particles will collide the rate of change of the l'th floc size class due to coagulation in a general form is given by (*e.g. Jackson* [1995], *Malcharek* [1995]):

$$[\partial_t \bar{\phi}_l]^+ = \frac{1}{2} \sum_{i+j=l} \alpha ij \beta_{ij} \bar{\phi}_i \bar{\phi}_j - \bar{\phi}_l \sum_{i=1}^{\infty} \alpha_{il} \beta_{il} \bar{\phi}_i, \tag{52}$$

The first term in the above equation represents the rate at which collisions of particles of floc size classes i and j occur to form a new particle of floc size class l. The second term expresses the rate of loss of particles $\bar{\phi}_l$ due to the collision. β_{ij} is denotes the probability of collision of particles i and j and α_{ij} is the probability that they stick together after colliding.

Accordingly the rate of loss of the l'th floc size class $\bar{\phi}_l$ due to mechanical erosion (*e.g.* shear stress) of particles can be described as follows (*e.g. Malcharek* [1995]):

$$[\partial_t \bar{\phi}_l]^- = -\eta_k \bar{\phi}_l + \sum_{j=l+1}^{\infty} \eta_j \gamma_{jl} \bar{\phi}_j - \bar{\phi}_k \sum_{i=1}^{\infty} \theta_{ik} \beta_{il} \bar{\phi}_i + \sum_{j=l+1}^{\infty} \gamma_{il} \bar{\phi}_j \sum_{i=1}^{\infty} \theta_{ij} \beta_{ij} \bar{\phi}_i. \tag{53}$$

Here the first term on the right of the above equation describes the loss of floc size class l due to disaggregation by the action of shear stress, the second term on the right the increase of floc size class l due to the fragmentation of particles of the floc size class j containing flocs of bigger size, γ_{jl} and γ_{il} expresses the probability that the fragmentation of a bigger floc will create a smaller floc of floc size class l. The third and the fourth term on the right represent the gain and loss of particles of floc size class l due fragmentation by collision of particles of floc size classes i and j and i and l respectively. θ_{il} and θ_{ij} denote the probability that a particle of floc size class l or j will break up due to the collision with a particle of floc size class i. Again β_{il} and β_{ij} expresses the probability that particles of floc size classes i and l and i and j respectively will collide.

2.3 SPM Model (Version B, non-cohesive material)

This version of the model is designed to simulate erosion and sedimentation dynamics of non-cohesive material in shallow waters (*i.e.* depth < 30m) with strong tidal currents. The non-cohesive material is assumed to interact with the bed so that it is both eroded from the bottom and deposited on the sea floor. This requires a bottom boundary condition permitting material flux at the bed. The following conditions are implemented (i denotes the i'th SPM fraction):

1. Free Surface Boundary Condition:

$$\left[\bar{\phi}_i w_{s,i} - \frac{\nu_t}{\sigma_{\phi_i}} \partial_z \bar{\phi}_i\right]_{z=0} = 0. \tag{54}$$

2. Bottom Boundary Condition:

$$\left[\bar{\phi}_i w_{s,i} - \frac{\nu_t}{\sigma_{\phi_i}} \partial_z \bar{\phi}_i\right]_{z=-H} = j_{s,i} + j_{e,i}. \tag{55}$$

where $j_{s,i}$ is calculated using a formula given by *Krone* [1962]:

$$\dot{j}_s = \begin{cases} \phi_{b,i} w_{s,i} \left(1 - (\frac{u_b^*}{u_{d,i}^*})^2\right) & \text{for} \quad u_b^* < u_{d,i}^*, \\ 0 & \text{otherwise.} \end{cases}$$

$w_{s,i}$ is calculated according to (49), u_b^* denotes the bottom friction velocity (in ms^{-1}), $\phi_{b,i} = \phi(z_{b,i}, t)$ is the bottom SPM concentration and $u_{d,i}^*$ is a critical bottom friction velocity beyond which no deposition is possible. For values of u_b^* smaller than $u_{d,i}^*$ sedimentation is enabled.

$j_{e,i}$ is calculated in accordance with *Partheniades* [1963]:

$$j_{e,i} = \begin{cases} M_e \left(\frac{u_b^* - u_{e,i}^*}{u_{e,i}^*}\right), & u_b^* > u_{e,i}^*, \\ 0, & \text{otherwise.} \end{cases}$$

Here, M_e is a constant with $M_e = 0.0001$, $u_{e,i}^*$ represents the critical bottom friction velocity which must be exceeded to enable erosion of sediment from the bed. In both the deposition and erosion cases the values of $u_{d,i}^*$ and $u_{e,i}^*$ were chosen to be 0.028 ms^{-1}. This corresponds to sinking velocities greater than 0.0005 ms^{-1} which is the case in our investigations.

In this model (version B) the bed thickness and water level are not time invariant so that the spatial domain of integration is also variable as it is adapted to the actual water depth each time step. In the present model version, the water depth function $H(t)$ is given as

$$H(t) = h_\zeta(t) + h_b(t) + \bar{H}$$

where

$$h_\zeta(t) = A_G \cos\left(\frac{2\pi}{T_G} t + \varphi_G\right)$$

with $h_\zeta(t)$ denoting the tidally induced deviation of sea surface from the the undisturbed water depth $\bar{H}$ [m]. A_G is the M_2 tidal amplitude, T_G the M_2 tidal period, φ_G the phase of the M_2 tide and t the time in seconds. $h_b(t)$ is the time dependent bottom thickness in meter.

3 Numerical Solution

3.1 General Aspects

Special emphasis has been placed on model development in order to obtain a fast, robust and highly efficient code so that at least one annual cycle

can be simulated on a personal computer in reasonable runtime. A 63 day simulation (time step = 600s) on a 66 MHz 486-DX2 processor takes about 10 minutes. The same task run on an IBM RISC 6000 is completed in about 1 minute.

3.2 Discretization in Space and Time

The discretization of the diffusion equations in (1) is conducted using a three-point, two-layer finite-difference scheme on a staggered grid based on the methods of *Baumert & Radach* [1992] and *Burchard & Baumert* [1995]. For improved spatial resolution in the near-bed region, the vertical axis is discretized with a non-equidistant grid. The horizontal pressure gradients in (1) are forced by the M_2 and S_2 tidal signals at the given geographical position according to equations (4) and (5).

3.3 Numerical Treatment of the Boundary Conditions

In this section the approximations used for the boundary conditions are described in a general form. Both kinds are used in this model boundary conditions of the first (44)–(46) and of the second kind (48)-(55). First the boundary condition of the second kind are dealt with, after that the boundary condition of the first kind is shown.

For all state variables with the exception of the SPM equation (the features of the SPM equation are described in chapter 3.5) the underlying differential equation reads in a general notation:

$$\partial_t Y = \partial_z \left(\nu \partial_z Y\right) + \Psi(z,t) \tag{56}$$

Y denotes the state variable under consideration, ν the turbulent viscosity and $\Psi(z,t)$ represents a general source function. The corresponding free surface and bottom boundary conditions are formulated in a general form as

$$-\nu \partial_z Y|_{z=0} = L_0(t) - K_0(t)\, Y|_{z=0} \tag{57}$$

and

$$\nu \partial_z Y|_{z=-H} = L_H(t) - K_H(t)\, Y|_{z=-H} \tag{58}$$

respectively with given relations $\nu(z,t), K_0(t), L_0(t)$ and $K_H(t), L_H(t)$ and the unknown function $Y(z,t)$. ν is found in both equation (56) and the boundary conditions (57) and (58).

To formulate an approximation for these boundary conditions, let the not necessarily uniform discretization step between the grid points $i+1$ and i be defined as $h_i := z_i - z_{i-1}$ with $i = 2..M$ and M the number of gridpoints. z_{i+1} and z_i represent the depth of the $i+1$ and i gridpoints respectively. Please notice that the indexing in this model is performed from the bottom to the surface, thus the discretization step at the free surface is given by $h_M := z_M - z_{M-1}$ with the corresponding step at the bottom boundary $h_2 := z_2 - z_1$. Here index 1 denotes the bottom value and index M the surface value of the variables under consideration and in the following '$\hat{}$' indicates unknown values on the new time level.

In a general form, the used tri-diagonal equation reads:

$$a_i \cdot \hat{Y}_{i+1} - c_i \cdot \hat{Y}_i + b_i \cdot \hat{Y}_{i-1} + d_i = 0 \tag{59}$$

where the indices $i-1$,i and $i+1$ refer to the corresponding grid point numbering with $i = 2, ..., M-1$. The coefficients a_i, b_i, c_i and d_i are known on the old time level. Their values depend on the applied discretization scheme. Here we used a fully implicit three point, two layer finite-difference scheme, which results in (τ is the integration time step and $t_1 := t_0 + \tau$):

$$a_i = -\nu_{(i-\frac{1}{2})}\frac{\tau}{h_i^2}, \quad b_i = -\nu_{(i+\frac{1}{2})}\frac{\tau}{h_i^2}, \quad c_i = 1 - a_i - b_i \quad \text{and} \quad d_i = Y_i + \Psi_i \cdot \tau. \tag{60}$$

At the boundaries (59) takes the form:
At the surface (z=0):

$$-c_M \cdot \hat{Y}_M + b_M \cdot \hat{Y}_{M-1} + d_M = 0 \tag{61}$$

and at the bottom (z=-H):

$$a_1 \cdot \hat{Y}_1 - c_1 \cdot \hat{Y}_2 + d_1 = 0. \tag{62}$$

In order to get suitable descriptions of the coefficients in (61) and (62) we discretize (57) and (58) in space only, to get the following approximations of second order:
At the free surface:

$$-\nu_{(M-\frac{1}{2})}\frac{\hat{Y}_{M-1} - \hat{Y}_M}{h_M} = L_0 - K_0\hat{Y}_M - \frac{h_M}{2}\left(\partial_t Y|_M - \Psi_M\right) \tag{63}$$

and at the bottom:

$$\nu_{(1+\frac{1}{2})}\frac{\hat{Y}_1-\hat{Y}_2}{h_2}=L_H-K_H\hat{Y}_1-\frac{h_2}{2}\left(\partial_t Y|_1-\Psi_1\right). \tag{64}$$

The time domain is, in accordance with the approach adopted for the differential equations, discretized fully implicit. Thus, the following approximations are valid:
At the free surface:

$$\frac{\hat{Y}_M-Y_M}{\tau}=\frac{2}{h_M}\Big(\nu_{(M-\frac{1}{2})}\frac{\hat{Y}_{M-1}-\hat{Y}_M}{h_M}+L_0-K_0\hat{Y}_M\Big)+\Psi_M \tag{65}$$

and, at the bottom:

$$\frac{\hat{Y}_1-Y_1}{\tau}=\frac{2}{h_2}\Big(-\nu_{(1+\frac{1}{2})}\frac{\hat{Y}_1-\hat{Y}_2}{h_2}+L_H-K_H\hat{Y}_1\Big)+\Psi_1. \tag{66}$$

Rearrangement of equations (65) and (66) gives the following expressions for the boundary conditions of the second kind as a second order approximation:
For the free surface

$$\left.\begin{aligned}\hat{Y}_M &= \kappa_1\hat{Y}_{M-1}+\mu_1\\ \kappa_1 &:= \frac{2\nu_{(M-\frac{1}{2})}\tau}{h_M^2}\Big/\delta_1\\ \mu_1 &:= \Big(Y_M+\frac{2L_0\tau}{h_M}+\tau\Psi_M\Big)\Big/\delta_1\\ \delta_1 &:= 1+\frac{2\nu_{(M-\frac{1}{2})}\tau}{h_M^2}+\frac{2K_0\tau}{h_M}\end{aligned}\right\} \tag{67}$$

with the corresponding coefficients c_M, b_M and d_M calculated as:

$$\left.\begin{aligned}b_M &= -\kappa_1\cdot\delta_1 &&= -\frac{2\nu_{(M-\frac{1}{2})}\tau}{h_M^2}\\ c_M &= \delta_1 &&= 1-b_M+\frac{2K_0\tau}{h_M}\\ d_M &= \mu_1\cdot\delta_1 &&= Y_M+\frac{2L_0\tau}{h_M}+\tau\Psi_M\end{aligned}\right\} \tag{68}$$

The bottom boundary condition results in:

$$\left.\begin{aligned} \hat{Y}_1 &= \kappa_2 \hat{Y}_2 + \mu_2 \\ \kappa_2 &:= \frac{2\nu_{(1+\frac{1}{2})^\tau}}{h_2^2} \Big/ \delta_2 \\ \mu_2 &:= \left(Y_1 + \frac{2L_H\tau}{h_2} + \tau\Psi_1\right) \Big/ \delta_2 \\ \delta_2 &:= 1 + \frac{2\nu_{(1+\frac{1}{2})^\tau}}{h_2^2} + \frac{2K_H\tau}{h_2}, \end{aligned}\right\} \tag{69}$$

with the corresponding coefficients a_1, c_1 and d_1 calculated as:

$$\left.\begin{aligned} a_1 &= -\kappa_2 \cdot \delta_2 &&= -\frac{2\nu_{(1+\frac{1}{2})^\tau}}{h_2^2} \\ c_1 &= \delta_2 &&= 1 - a_1 + \frac{2K_H\tau}{h_2} \\ d_1 &= \mu_2 \cdot \delta_2 &&= Y_1 + \frac{2L_H\tau}{h_2} + \tau\Psi_1. \end{aligned}\right\} \tag{70}$$

In terms of (67) and (69) the used boundary conditions of the first kind read as follows:
For the free surface

$$\left.\begin{aligned} \hat{Y}_M &= \mu_1 \\ \kappa_1 &:= 0 \\ \mu_1 &:= Y_M^0 \\ \delta_1 &:= 1, \end{aligned}\right\} \tag{71}$$

from which follows, that $c_M = 1$, $b_M = 0$ and $d_M = Y_M^0$.
For the bottom boundary one obtains

$$\left.\begin{aligned} \hat{Y}_1 &= \mu_2 \\ \kappa_2 &:= 0 \\ \mu_2 &:= Y_1^0 \\ \delta_2 &:= 1, \end{aligned}\right\} \tag{72}$$

with $a_1 = 0$, $c_1 = 1$ and $d_1 = Y_1^0$ and Y_M^0 and Y_1^0 denoting always known values of Y at the surface and the bottom boundary, respectively.

Equations (67)-(72) are part of a linear system, the solution of which gives the values of state variable Y throughout the water column.

3.4 Numerical Treatment of the TKE-Equation

In order to improve the numerical stability of the discrete algorithm we described (43) by a continuous function, rather than by a stepwise function. In relation to the general discrete form (67) the conditions in (43) are equivalent to the statements that (note that the discrete form of the TKE-equation boundary condition is a first order approximation of (43) and t denotes the time)

$$\hat{k}_M = \hat{k}_{M-1} \quad \text{or} \quad \kappa_1 = 1 \quad \text{and} \quad \mu_1 = 0 \quad \text{if} \quad k_M > u_s^{*2}/\sqrt{c_\mu}$$

and

$$\hat{k}_M = u_s^{*2}/\sqrt{c_\mu} \quad \text{or} \quad \kappa_1 = 0 \quad \text{and} \quad \mu_1 = u_s^{*2}/\sqrt{c_\mu} \quad \text{if} \quad k_M <= u_s^{*2}/\sqrt{c_\mu}.$$

This behaviour can be approximated asymptotically by the following relations for κ_1 and μ_1:

$$\kappa_1 = k^* \cdot \frac{k^*}{k_M + k^*} \qquad \text{and} \qquad \mu_1 = 1 - \frac{k^*}{k_M + k^*},$$

whith $k^* = u_s^{*2}/\sqrt{c_\mu}$.

3.5 Numerical Treatment of the SPM Equation

On discretization of the SPM equation, one has to consider the magnitude of the cell Peclet number. This is defined as the ratio of the advective (sinking) term to the diffusive flux term of SPM ($Pe_i = \frac{w_s\, h}{\nu_t}$). For smaller cell Peclet numbers (*i.e.* < 2) central differencing of the advective term is a reasonable approach. However, for bigger cell Peclet numbers (>2), an upwind scheme is necessary in order to maintain stability of the solution. For these reasons, the SPM budget equation in the model was defined using the control volume approach applying a power law interpolation scheme as described by *Patankar* [1980]. This scheme takes care of both smaller and larger cell Peclet numbers. Since upwind schemes are highly diffusive (which becomes especially evident in regions of low physical diffusion), the advective term

was discretized using the hybrid linear/parabolic approximation (HLPA) scheme proposed by *Zhu* [1991]. This approach constitutes a higher order upwind scheme and exhibits much reduced numerical diffusion. Note that in the following, we use ϕ instead of $\bar{\phi}$, but still refer to the ensemble averaged variable. In this chapter the discretizised SPM equation is described in a general form, thus we omit the index indicating the SPM fraction. Here in case of the SPM equation the coefficients in (59) are given by:

$$a_i = D_{i+\frac{1}{2}} \cdot A\left(\left|Pe_{i+\frac{1}{2}}\right|\right) + \max\left[-F_{i+\frac{1}{2}}, 0\right] \tag{73}$$

$$b_i = D_{i-\frac{1}{2}} \cdot A\left(\left|Pe_{i-\frac{1}{2}}\right|\right) + \max\left[F_{i-\frac{1}{2}}, 0\right] \tag{74}$$

$$c_i^0 = \frac{h_i + h_{i-1}}{2 \cdot \tau} \tag{75}$$

$$c_i = a_i + b_i + c_i^0 + \left(F_{i+\frac{1}{2}} - F_{i-\frac{1}{2}}\right) \tag{76}$$

where

$$D_{i\pm\frac{1}{2}} = \frac{\nu_{t_{i\pm\frac{1}{2}}}}{h_{i\pm\frac{1}{2}}}, \qquad F_{i\pm\frac{1}{2}} = w_{s_{i\pm\frac{1}{2}}} \quad \text{and} \quad Pe_{i\pm\frac{1}{2}} = \frac{F_{i\pm\frac{1}{2}}}{D_{i\pm\frac{1}{2}}} \tag{77}$$

The applied power law as published by *Patankar* [1980] is

$$A\left(|X|\right) = \max\left((1 - 0.1 \cdot |X|)^5, 0\right) \tag{78}$$

with which the corresponding terms in equations (73) and (74) can be obtained.

If $F_{i+\frac{1}{2}} > 0$

$$F^*_{i+\frac{1}{2}} = \gamma_{i+\frac{1}{2}}(\phi^n_{i+1} - \phi^n_i)\left(\frac{\phi^n_i - \phi^n_{i-1}}{\phi^n_{i+1} - \phi^n_{i-1}}\right) \tag{79}$$

with

$$\gamma_{i+\frac{1}{2}} = \begin{cases} F_{i+\frac{1}{2}} & \text{if} \quad |\phi^n_{i-1} + \phi^n_{i+1} - 2\phi^n_i| < |\phi^n_{i+1} - \phi^n_{i-1}| \\ 0 & \text{otherwise} \end{cases}$$

If $F_{i+\frac{1}{2}} < 0$ then

$$F^*_{i+\frac{1}{2}} = \gamma_{i+\frac{1}{2}}(\phi^n_i - \phi^n_{i+1})\left(\frac{\phi^n_{i+1} - \phi^n_{i+2}}{\phi^n_i - \phi^n_{i+2}}\right) \tag{80}$$

with

$$\gamma_{i+\frac{1}{2}} = \begin{cases} F_{i+\frac{1}{2}} & \text{if} \quad |\phi_i^n + \phi_{i+2}^n - 2\phi_{i+1}^n| < |\phi_i^n - \phi_{i+2}^n| \\ 0 & \text{otherwise} \end{cases}$$

Corresponding expression for $F^*_{i-\frac{1}{2}}$ follow from (79) and (80) with $i - \frac{1}{2} = (i-1) + \frac{1}{2}$. Finally

$$d_i = c_i^0 \cdot \phi_i^n + F^*_{i-\frac{1}{2}} - F^*_{i+\frac{1}{2}} \tag{81}$$

The coefficients given by equations (73)-(76) and (81) are always known at the old time level. $D_{i\pm\frac{1}{2}}$ and $F_{i\pm\frac{1}{2}}$ denote the diffusive and convective fluxes of material respectively. The second and third terms on the right hand side of equation (81) can be regarded as an antidiffusive correction to the upwind scheme (*Zhu* [1991]). The power law scheme used here (equation (78)) requires a significant amount of computing time. However, it provides the most accurate solutions, closest to the analytical solutions.

4 Results and Discussion

In order to validate the discretization schemes (especially for the SPM equation), tests were conducted to compare the results of specific model runs with analytical solutions and also measured data. These tests have been carried out for both model versions A and B. For a comparison with measurements, we have used the data obtained during the FLEX'76 experiment. This dataset consists of measured temperature profiles for an assessment of the model's performance and also the meterological information required as model input.

In future, the model will be tested using the new datasets from the PROMIX'96 experiment in the Sylt-Rømø Bight and the Holderness experiments. These datasets will permit detailed insight into the model's ability to simulate microstructure properties of turbulent flow dynamics.

4.1 Model Results against Analytical Solutions

For these model tests, three different analytical solutions of the stationary SPM advection/diffusion equation were considered. Against each of these scenarios, we tested three different numerical schemes : the upwind scheme, the hybrid scheme derived by *Spalding* [1972] and the power law scheme. The three test cases consisted of:

1. Constant sinking velocity w_{s_0} and constant turbulent viscosity ν_{t_0}. Thus, we have the following analytical relation for ϕ

$$\phi(z) = a + be^{\frac{-w_{s_0}z}{\nu_{t_0}}} \tag{82}$$

with

$$b = \frac{\phi_H - \phi_0}{e^{Pe} - 1} \quad \text{and} \quad a = \phi_0 - b$$

where ϕ_H and ϕ_0 denote the SPM concentration at the bed and surface respectively. The water depth (H) was chosen as 20 m with 10 grid-points in the vertical. Sinking velocity and turbulent viscosity were set to w_{s_0} =-0.6 ms^{-1} and $\nu_{t_0} = 2$ m^{2}s^{-1} respectively. These assumptions lead to a constant $Pe = -6$. These specific values were chosen in order to enable us to distinguish differences in the behaviour of the applied discretization schemes. It is clear from Figure 1 that the closest fit to the analytical solution is provided by the power law scheme.

2. In the case of exponential behaviour for turbulent viscosity ($\nu_t(z) = \nu_{t_0}e^z$) and sinking velocity ($w_s(z) = -w_{s_0}e^z$) the analytical solution for ϕ is given by

$$\phi(z) = ae^{-z} + be^{-\frac{w_{s_0}z}{\nu_{t_0}}} \tag{83}$$

with the coefficients

$$b = \frac{\phi_0 e^{-H} - \phi_H}{e^{-H} - e^{-\frac{w_{s_0}H}{\nu_{t_0}}}} \quad \text{and} \quad a = \phi_0 - b$$

In this case w_{s_0} =-18 ms^{-1} and ν_{t_0} =3 m^{2}s^{-1} respectively, leading to a cell Peclet number of $Pe = -12$. As with the previous case, the power law model scheme provided exhibited the smallest deviation from the analytical solution. A comparison of the various results is shown in Figure 2.

3. Assuming a depth dependent sinking velocity and turbulent viscosity with $w_s(z) = -w_{s_0}(z+1)$ and $\nu_t(z) = \nu_{t_0}(z+1)^2$, we get for ϕ

$$\phi(z) = \frac{a}{1+z} + b(1+z)^{-\frac{w_{s_0}}{\nu_{t_0}}} \tag{84}$$

with

$$b = \frac{\phi_H(1+H) - \phi_0}{(1+H)^{\frac{\nu_{t_0} - w_{s_0}}{\nu_{t_0}}} - 1} \quad \text{and} \quad a = \phi_0 - b$$

The surface values were set to w_{s_0} =-1.0 ms^{-1} and ν_{t_0} =2 $\mathrm{m}^2\mathrm{s}^{-1}$ respectively. In this case the cell Peclet number is not constant.

Figure 3 shows that, as before, the power law scheme is the most appropriate for the considered advection/diffusion equation.

4.2 Model Results Against Measured Data

In order to validate the model against measured data, simulations at the site of the Fladenground Experiment [1976] (FLEX'76) were carried out. The FLEX'76 dataset contains both the meteorological data required for the model forcing as well as measured temperature profiles which can be used to validate the model results (see *Burchard & Baumert* [1995]). In addition to comparison of the isopleth diagrams for the temperature field, the rms error of temperature over the upper half of the water column serves as a useful measure of the model's performance. Both of the isopleth diagrams (figures 4 and 5) and the computed rms error of 0.23 show that the model has been well designed and implemented. These results are comparable with those of other authors (*e.g. Burchard & Baumert* [1995]). All of the well known events (the onset of stratification on the 110th day and the storm around the 134th day) observed during FLEX'76 are reproduced by the generic model.

As soon as the required data is available, further applications of the 1-d model will be carried out at the site of the Holderness experiments.

4.3 Results of SPM Simulations

In order to test the two SPM modules used in versions A and B, we have constructed suitable test cases for each approach.

4.3.1 Results for Version A (cohesive sediments)

For this particular version of the model, the SPM population was assumed to consist of flocs of diameter 40 μ m with a sinking velocity of $1.5 \cdot 10^{-3}\mathrm{ms}^{-1}$ and density of 1005 kgm^{-3}. The initial floc concentration was set to 0.1 kgm^{-3}. The vertical grid was uniform with 120 grid points and a water depth of 145m (corresponding with the FLEX'76 dataset). The integration timestep for the run was set to 150secs and the tidal forcing was configured such that on springs the currents peaked at around $1.2\mathrm{ms}^{-1}$.

Figure 5 shows the model results for two tidal periods. Floc concentration is shown in sub-diagram 5d. The isopleths display a clear tidal signal. Figure 5e shows contours the cell Peclet number *i.e.* the ratio of convective and diffusive fluxes. Near to the boundaries, convective processes dominate whereas diffusive processes are more important in the interior of the water column. A similar feature can also be identified from the TKE, dissipation rate and eddy viscosity contour plots. There is a clear tidal signal in the TKE results with the strongest variation found in the near bed region. It is this turbulent energy that is resulting in the transport of SPM into the interior of the water column.

4.3.2 Results for Version B (non-cohesive sediments)

A shallow tidal channel with a mean depth of 15m was chosen as the test case for this version of the model. Varying depth (and layer thickness) is included in the model to incorporate a tidal range of approximately 2m and variable bed thickness due to bottom exchange processes. The SPM population was assumed to be sand with a grain diameter of $100\,\mu$m, sinking velocity $10^{-2}\mathrm{ms}^{-1}$ and a density of $2650\,\mathrm{kg\,m}^{-3}$. The non-regular grid was chosen for increased resolution in the near bed region. Tidal velocities peaked at $3\mathrm{ms}^{-1}$.

The model results (Fig. 6) cover two adjacent tidal periods and clearly display the fundamental dynamics of the system. The onset of resuspension of bed material triggered by strong tidal action is clearly visible. Due to the effects of high SPM concentration on the water density, the continuous resuspension and subsequent upward diffusive transport of this material leads to relatively sharp density gradients close to the bed. As with the previous run, the cell Peclet number results (Fig. 6e) indicate that convection is dominant near the boundary whereas diffusion becomes the important process in the interior of the water column.

5 Technical Aspects

At present, the model is coded using Borland's Pascal 7.0 package. It subsequently runs on an IBM compatible personal computer under DOS (version 3.2 or better). A second model version is designed for use on UNIX machines (*e.g.* IBM-RISC). To compile the code on an IBM-RISC machine requires at least the IBM-AIX XL Pascal compiler (version 1.1). For both these model versions, the run parameters are specified using corresponding control files. These control files (`CONTROL.DAT`) assume the following format:

```
North Sea        { Comment, up to 12 Characters ...                          }
    2            { 1: Save single point time series; 2: 1 plus profiles      }
FLEX____         { Name of the forcing data file; 8 Char,;(Ext,:'dat' implied)}
dxe.t            { Grid file name   (8 Char. + 3 Char. extension)            }
    63           { Number of days for which forcing data exist               }
   58.55         { Latitude in degree                                        }
  150.0          { Water depth [m]                                           }
  120            { Number of grid points used                                }
  600.0          { Integration time step [s]                                 }
      1    .     { Flag: 0 - run without SPM, 1: run with SPM                }
                 { blank                                                     }
  -0.275         { Phase of the M2-tide                                      }
  -0.275         { Phase of the S2-tide                                      }
  4.0e-05        { Amplitude 1 of the M2-tide                                }
  5.0e-05        { Amplitude 2 of the M2-tide                                }
  4.0e-05        { Amplitude 1 of the S2-tide                                }
  5.0e-05        { Amplitude 2 of the S2-tide                                }
 435000          { Lag netween model time and tidal phase                    }
                 { blank                                                     }
  2650           { Density of sediment [kg/m^3]                              }
  -0.001         { Sinking velocity [m/s]                                    }
  2650           { Maximum concentration [kg/m^3]                            }
  0.1            { Start value of concentration [kg/m^3]                     }
```

Three additional lines are included in the control file for use with model version B:

```
  0.028          { Critical bottom frict. vel. for sediment                  }
  0.030          { Critical bottom frict. vel. for erosion                   }
  1.0            { Max. depth of erosion [m]                                 }
```

The first line in the forcing data file contains the initial water temperature, which is considered to be homogeneous. This is followed by the external forcing data at one hour intervals. Table 2 describes the form of the external forcing datasets.

The data is assumed to be valid at a height of 10m above the sea level and are taken as the mean values above the sea surface.

The model results are saved in three files which have the same name as the forcing data file but have differing extensions. The file with extension *.TIM contains single point time series, whereas those with extensions *.PRF and *.PR2 contain timeseries of profiles of selected parameters. Parameter profiles are saved from surface to bed. In addition to the velocity components, temperature, salinity and density, the model output includes information regarding the turbulent flow field. The microstructure parameters are listed in Table 3.

Each of the three output files starts with a header which contains specified information for the model run. An example of such a header is given below

```
North Sea
Latitude        =       58.9160 degrees north
Water depth     =       150.0 m

Forcing         =       FLEX____.DAT

DT              =       600.0 s


      t             H     T_s      T_1/2      T_b
     [d]           [m]   [ C]       [ C]     [ C]  ....
-------------------------------------------------
    1.003          0.9   6.13       6.21     6.22
    2.005          0.0   6.07       6.15     6.16
     etc.
      ...
```

In this file, the first column is the time in days, the second contains the top layer mixed depth [m] and the third to fifth columns record the surface,

Column	Parameter	Unit
1	East–West component of wind stress	m^2s^{-2}
2	North–South component of wind stress	m^2s^{-2}
3	Global radiation	$Jm^{-2}s^{-1}$
4	Net turbulent heat flux at the sea surface	$Jm^{-2}s^{-1}$

Table 2: Columns of the forcing dataset

depth-mean and bottom temperatures respectively.

All of the above mentioned model data can easily be processes and visualised using customary PC graphics tools.

Symbol	Name	Unit	Calculation	Comment
ν_t	Eddy viscosity	$m^2 s^{-1}$	$\nu_t = c_\mu \frac{k^2}{\epsilon}$	Turbulent viscosity
C_x	Cox number	-	$C_x = \frac{\nu_t}{\sigma_t D_t}$	Ratio of turbulent to molecular heat conductivity
E_k	Local Ekman number	-	$E_k = \frac{\nu_t}{f H_w}$	Ratio of the friction to the Coriolis term
l_{BS}	Batchelor scale for salinity	$[m]$	$l_{BS} = \sqrt[4]{\frac{\nu D_s^2}{\epsilon}}$	Length scale for the smallest possible haline inhomogeneities
l_{BT}	Batchelor scale for temperature	$[m]$	$l_{BT} = \sqrt[4]{\frac{\nu D_t^2}{\epsilon}}$	Length scale for the smallest possible thermal inhomogeneities
l_k	Kolmogorov length scale	$[m]$	$l_k = \sqrt[4]{\frac{\nu^3}{\epsilon}}$	Lenght scale of the smallest not dissipated eddies
l_l	Eddy length scale	$[m]$	$l_l = \frac{k^{\frac{3}{2}}}{\epsilon}$	Lenght scale of the energy containing eddies
l_o	Ozmidov length scale	$[m]$	$l_o = \sqrt{\frac{\epsilon}{N^3}}$	Maximum vertical extension of turbulent eddies
Re	Local turbulent Reynolds number	-	$Re = \frac{\sqrt{k} l_l}{\nu_t}$	Measure of the dynamical condition (turbulent or laminar)
Re_b	Buoyancy Reynolds number	-	$Re_b = \frac{\epsilon}{\nu N^2}$	Measure of the dynamical condition (turbulent or laminar)
R_s	Stability ratio	-	$R_s = \left(\frac{\beta_s}{\alpha_t} \frac{\partial_z S}{\partial_z T}\right)^{\pm 1}$	Measure of he local thermohaline stability. +1(-1): salinity or (temperature) stabilised.
Rf	Flux Richardson number	-	$Rf = -\frac{G}{P}$	Measure of the stratification stability
Rg	Gradient Richardson number	-	$Rg = -\frac{N^2}{(\partial_z \bar{u})^2 + (\partial_z \bar{v})^2}$	Measure of the stratification stability
τ_m	Makro time scale of turbulence	$[s]$	$\tau_m = \frac{\nu_t}{k}$	Time scale of tubulent eddies
τ_k	Kolmogorov micro time scale of turbulence	$[s]$	$\tau_k = \frac{l_k}{\sqrt{k}}$	Time scale of the smallest not disspated eddies

Table 3: Micro structure data, which are included in the model output. D_t and D_s are the molecular diffusion coefficient for heat and salinity respectively [m^2/s], H_w is the water depth in m and α_t and β_s are the thermal and saline expansion coefficents [1/C] and salt [1/psu], respectively.

Acknowledgements

We would like to thank Prof. Jürgen Sündermann for his advice and persisting interest and Prof. Gisbert Stoyan for valuable discussions on theoretical aspects of the used numerical schemes. B. Szilagyi was supported by the Gottlieb Daimler- und Karl Benz-Stiftung through grant no. 02-06/96.

References

Baumert, H. and G. Radach (1992) - Hysteresis of turbulent kinetic energy in nonrotational tidal flows: a model study. *J. Geophys. Res.* Vol. **97**, 3669 - 3677.

Burchard, H. and H. Baumert (1995) - On the performance of a mixed-layer model based on the k-ϵ turbulence closure. *J. Geophys. Res.* Vol. **100**, C5, 8523 - 8540.

Busch, N.E. (1977) - Fluxes in the surface boundary layer over the sea. In: Modelling and Prediction of the Upper Layers of the Ocean (E.B. Kraus, ed.), Pergamon, 72 - 91.

Friedrich, H., Kochergin, K.P., Klimok, V.I., Protasov, A.V. and V.A. Sukhorukov (1981) - Numerical experiments with the upper layer ocean model (in Russ.). Meteorol. i Gidrol. No. **7**, 77 - 85.

Jackson, G. A. (1995) - Comparing observed changes in particle size spectra with those predicted using coagulation theory. *Deep Sea Res.* II, Vol. **42**, No. 1, 159 - 184.

Kiøboe, T., Lundsgaard, C., Olesen, M. and J. l. S. Hansen (1994) - Aggregation and sedimentation processes during a spring phytoplankton bloom: A field experiment to test coagulation theory. *J. Mar. Res.*, **52**, 297 - 323.

Kolmogorov, A.N. (1942) - Equations of turbulent motion on an incompressible fluid. *Izv. Akad. Nauk. SSSR Ser. Fiz., 1 - 2*, 56 - 58. (English translation, *Mech. Eng. Dept. Rept.* ON/6, Imperial College, London, 1968.)

Kondo, J. (1975) - Air-sea bulk transfer coefficients in diabatic conditions. *Boundary Layer Meteorol.*, **9**, 91 - 112.

Kondratyev, K.Y. (1969) - Radiation in the Atmosphere. Academic Press, N.Y.

Krone, R. B. (1962) - Flume studies of the transport of sediment in estuarial shoaling processes. Final report. Hydrolic eng. lab., University of California, Berkley.

Malcharek, A. (1995) - Mathematische Modellierung von Strömungen und Stofftransportprozessen in Ästuaren. Doktorarbeit, Fachbereich Bauingenieur- und Vermessungswesen der Universität Hannover, Hannover, Germany, 199 S.

Möller, F. (1973) - Einführung in die Meteorologie, Physik der Atmosphäre Teil I. BI Wissenschaftsverlag Band 276.

Munk, W.H. and E.R. Anderson (1948) - Notes on the theory of the ther-

mocline. *J. Mar. Res.*, **3**, 276 - 295.
Oliver, D.R. (1961) - The sedimentation suspension of closely-sized sperical particles. *Chem. Eng. Science*, Vol. **15**, 230 - 242.
Partheniades, A. (1965) - Erosion and Deposition of cohesive soils. *J. of the Hydr. Div. ASCE*, Vol. **91**, No. HY 1.
Patankar, S. (1980) - Numerical heat transfer and fluid flow. Hemisphere Publishing Corporation, New York, pp. 197.
Paulson, A. and J.J. Simpson (1977) - Irradiance measurements in the upper ocean. *J. Phys. Oceanogr.*, **7**, 952 - 956.
Prandtl, L. (1945) - Über ein neues Formelsystem für die ausgebildete Turbulenz. *Nachr. Akad. Wiss. Göttingen Math. Phys. Klasse,* **6**.
Reneger, M. (1992) - Deckschichtmodellierung an ausgewählten Standorten in der Nordsee mit dem van-Aken-Modell. Diplomarbeit FB Geowissenschaften Univ. Hamburg, 131 S.
Rodi, W. (1980) - Turbulence models and their application in hydraulics. Report, Int. Assoc. for Hydraul. Res., Delft, Netherlands.
Samarskij, A. A. (1984) - Theorie der Differenzenverfahren. Akademische Verlagsgesellschaft Geest & Portig, Leipzig, Germany.
Sheng, Y. P., Villaret, C. (1989) - Modeling the effect of susoended sediment stratification on bottom exchange processes. *J. Geoph. Res.*, Vol. **94**, No. C10, 14.429 - 14.444.
Spalding, D. B. (1972) - A novel finite-difference formulation for differential expressions involving both first and second order derivatives, *Int. J. Numer. Methods Eng.*, **4**, 551 - 559.
Tennekes, H. and J.L. Lumley (1972) - A first Course in Turbulence, MIT Press, Cambridge, Mass.
van Rijn, L. C. (1993) - Principles of sediment transport in rivers, estuaries and coastal seas. Aqua Publications, Amsterdam, Netherlands.
Zhu, J. (1991) - A low-diffusive and oscillation-free convection scheme. *Comm. in Appl. Num. Meth.*, Vol. **7**, 225 - 232.

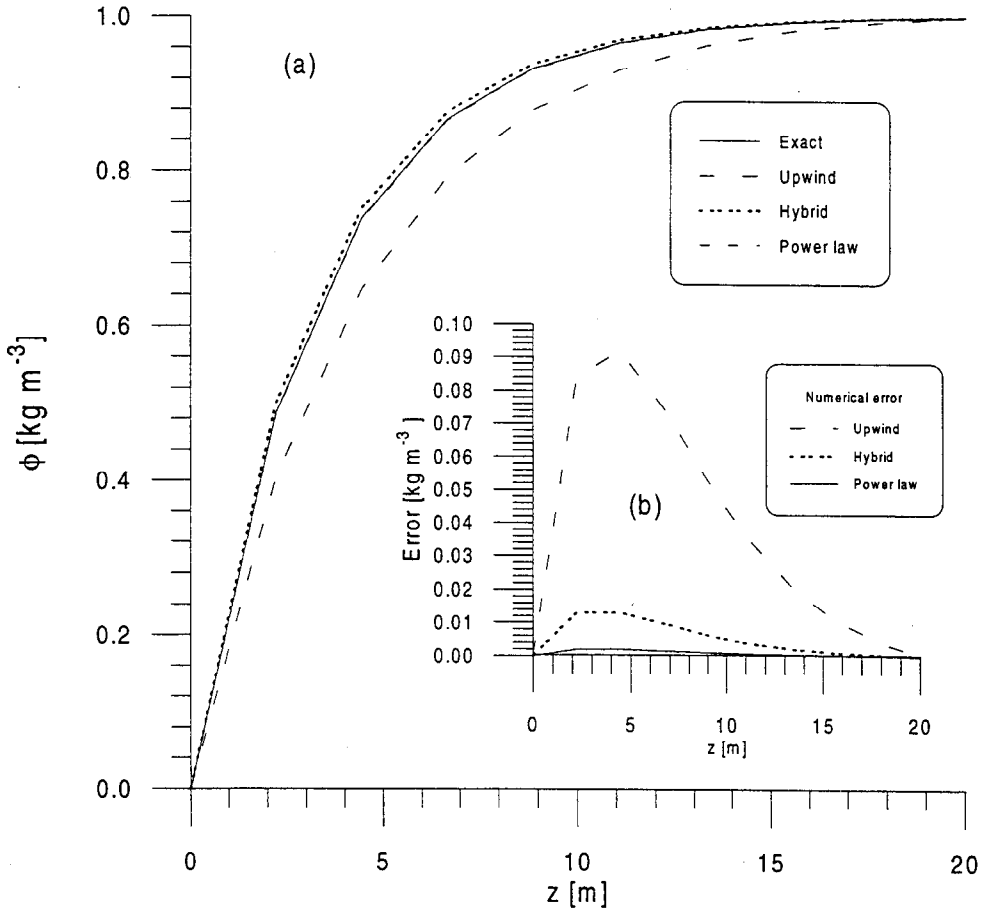

Fig. 1: Model results against analytical solution. Stationary solution with constant turbulent viscosity ν_t and sinking velocity $w_{s,m}$
(a) The vertical concentration profiles and (b) the abs. error between model results and analytical solution.

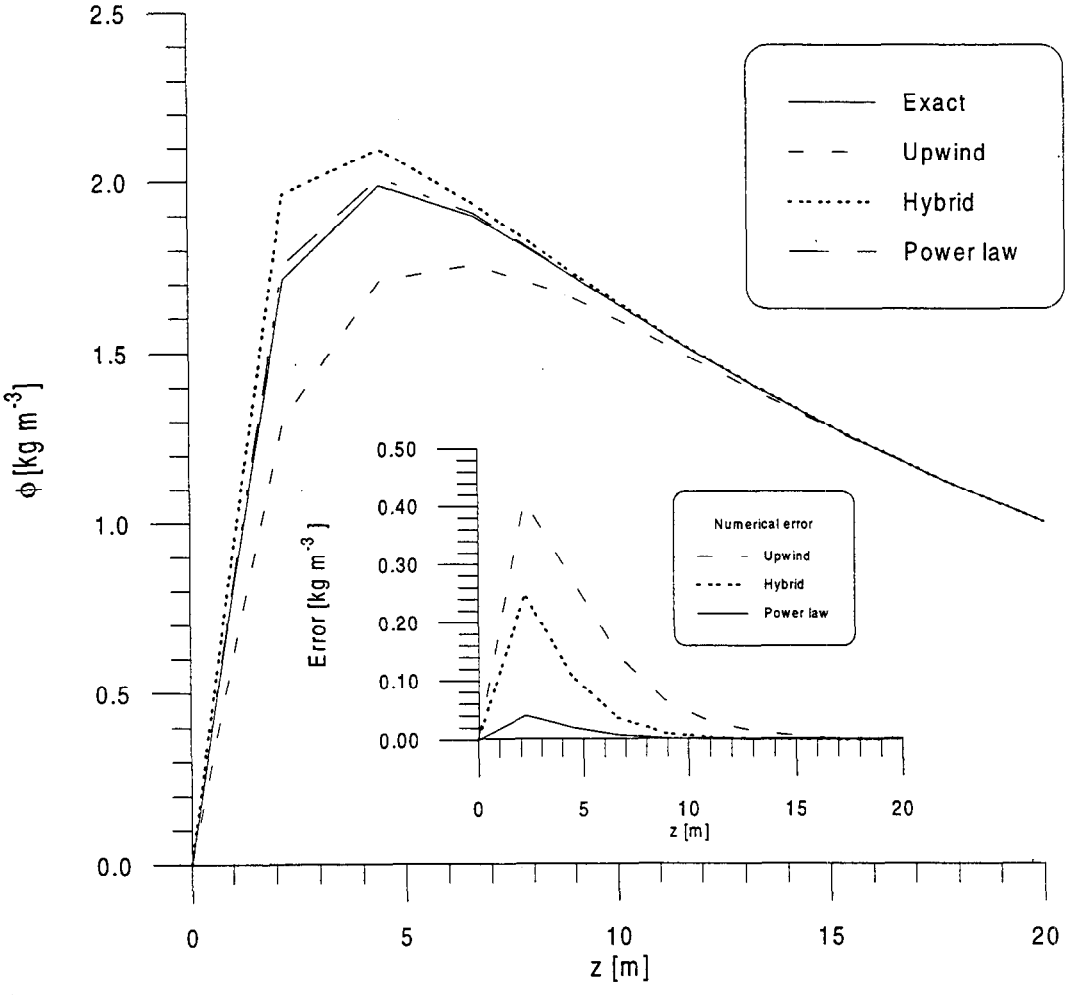

Fig. 2: Model results against analytical solution. Stationary solution with an exponential dependency of the turbulent viscosity ν_t and sinking velocity $w_{s,m}$

(a) The vertical concentration profiles and
(b) the abs. error between model results and analytical solution.

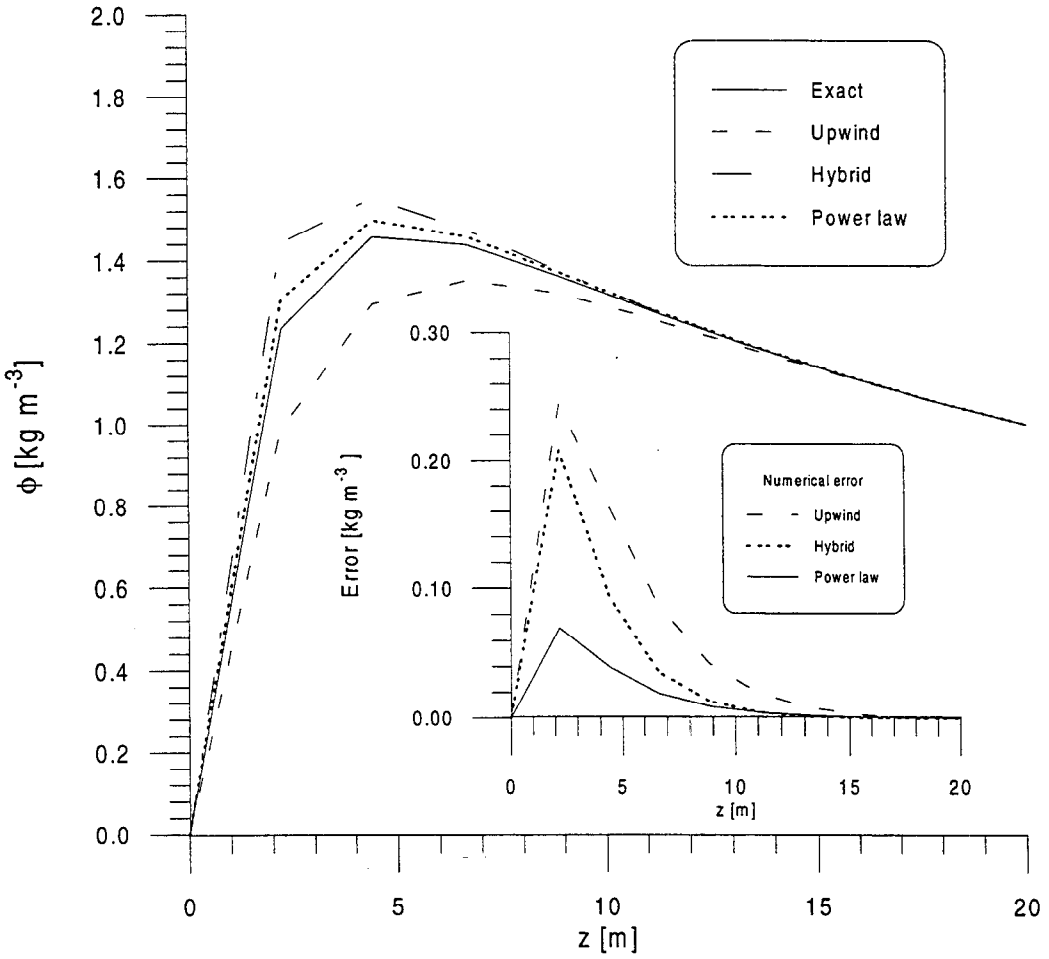

Fig. 3: Model results against analytical solution. Stationary solution with a depth dependend turbulent viscosity ν_t

and sinking velocity $w_{s,m}$ (see text)

(a) The vertical concentration profiles and

(b) the abs. error between model results and analytical solution.

(a)

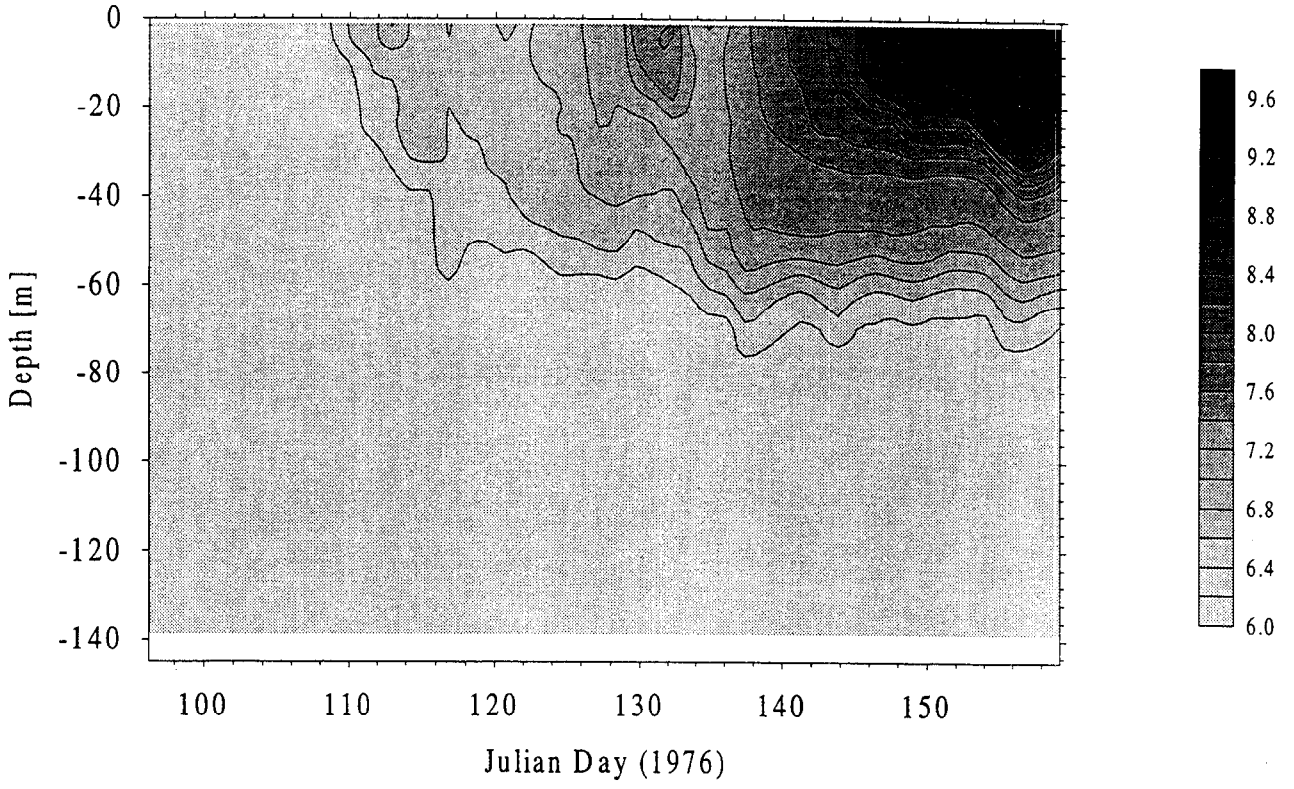

(b)

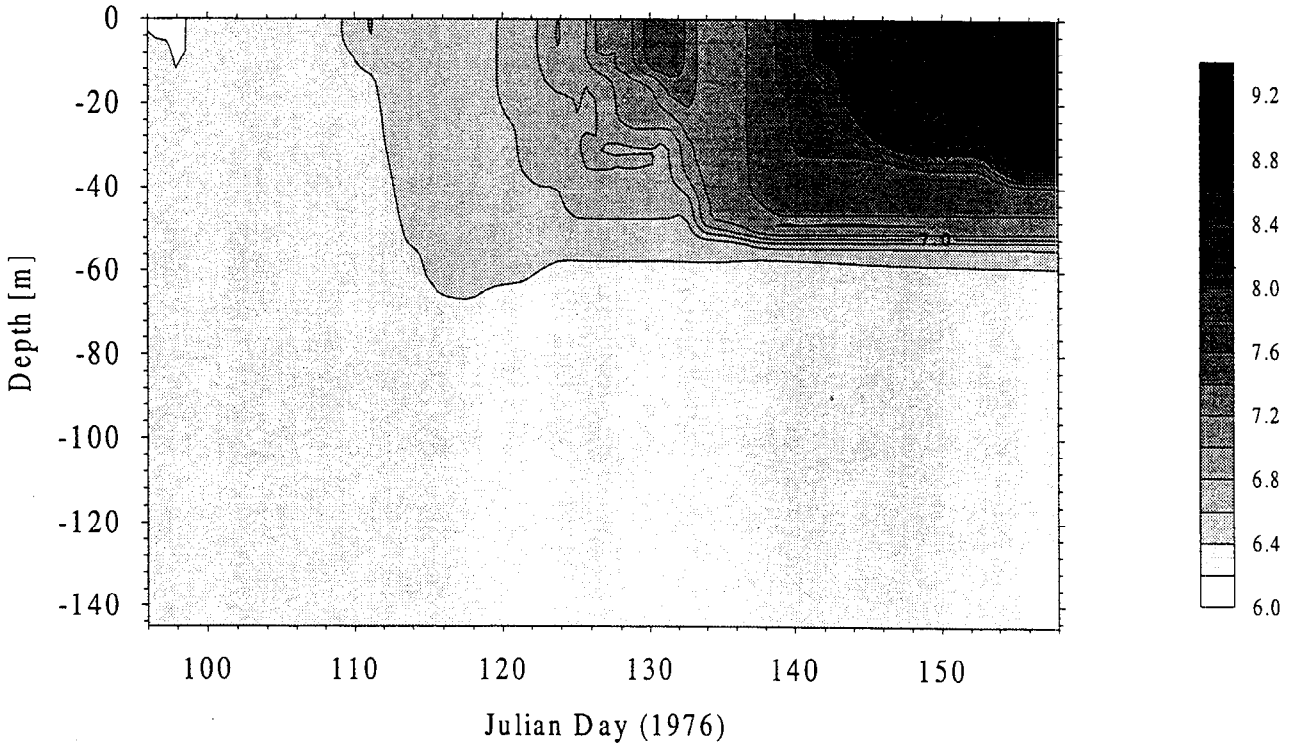

Fig. 4 : a) Isopleth diagram of measured temperatures and b) Isopleth diagram of simulated temperature distribution for FLEX'76 in °C.
Calculated with model version A .

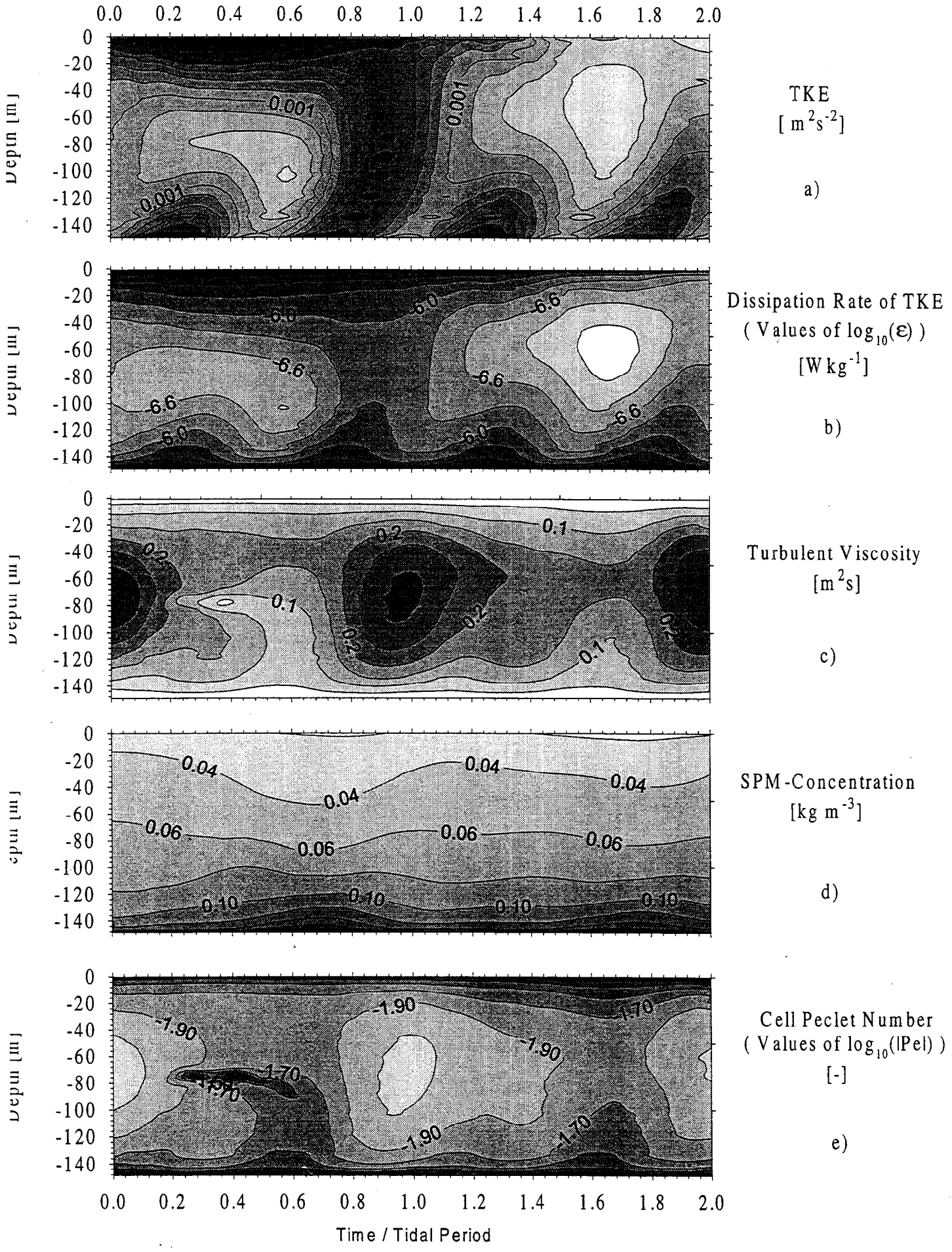

Fig 5: Isopleths diagrams of simulated a) TKE, b) dissipation rate of TKE, c) turbulent viscosity, d) SPM concentration and e) the cell Peclet number. Calculated with model version A.

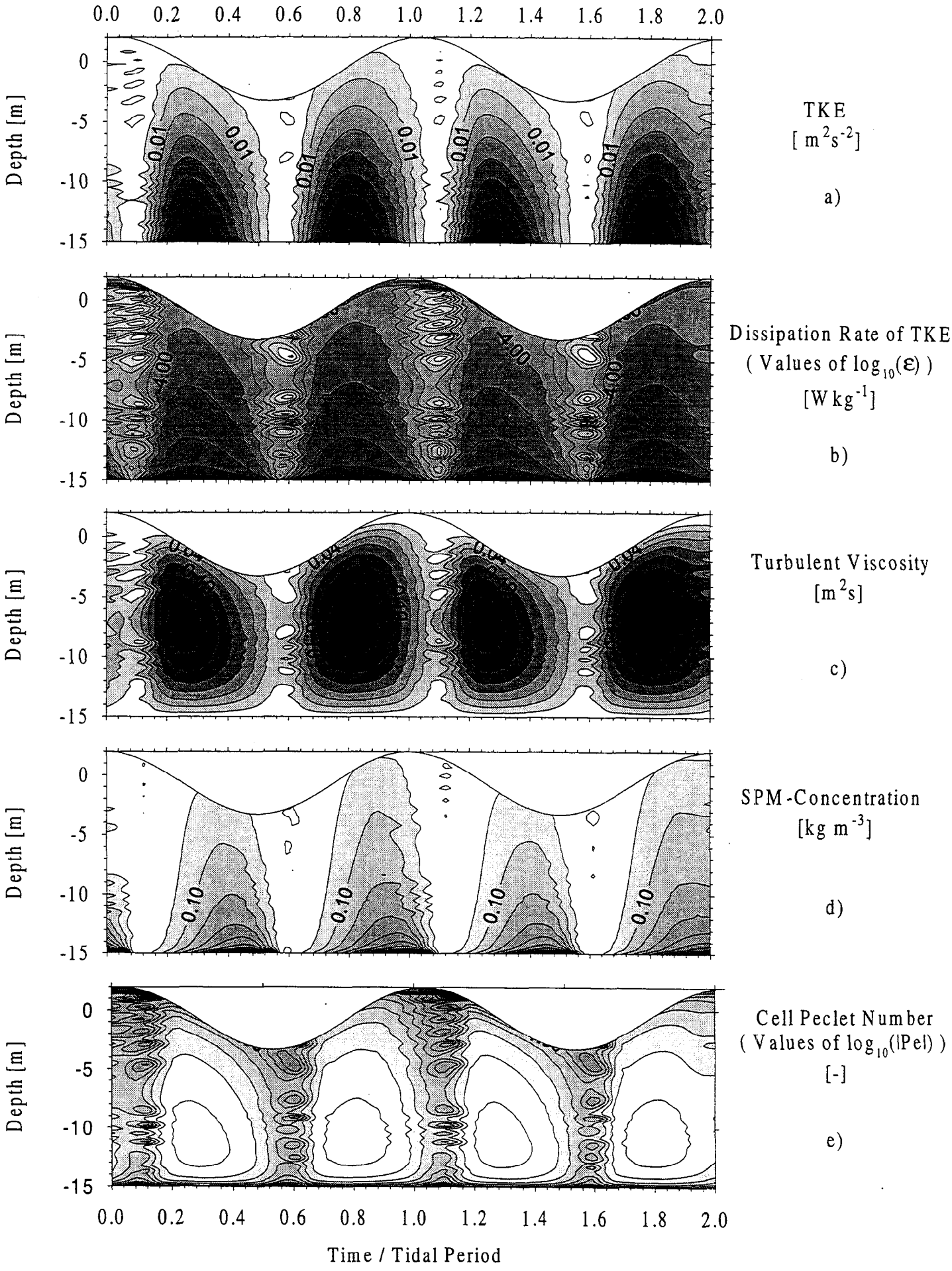

Fig. 6: Isopleths diagrams of distributions of(a) SPM, (b) turbulent viscosity, (c) TKE, (d) dissipation rate of TKE and (e) the cell Peclet number calculated with model version B.